16 Organic Semiconductors

Organic semiconductors are based on carbon compounds. The main structural difference from inorganic semiconductors is the bond based on sp^2 hybridization (cf. Sect. 2.2.3) as present in benzene (and graphite). Diamond, although consisting of 100% carbon, is not considered an organic semiconductor. We note that carbon can form further interesting structures based on sp^2 bonds, such as carbon nanotubes (Sect. 17.2), (single or few layer) graphene sheets (Sect. 17.1) rolled up to form cylinders, or fullerenes, e.g. soccer-ball-like molecules such as C_{60}.

In the 1980 Handbook on Semiconductors only a good ten pages were devoted to organic semiconductors [969]. Now several textbooks are available [970, 971] for a much more detailed treatment than given here.

16.1 Materials

16.1.1 Small Organic Molecules, Polymers

The prototype organic molecule is the benzene molecule with its ring-like structure (Fig. 2.8).

There is a large number of organic, semiconducting molecules that differs by the number of benzene rings (Fig. 16.1), the substitution of carbon atoms by nitrogen or sulfur (Fig. 16.2a,b), the polymerization (Fig. 16.2c) or the substitution of hydrogen atoms by side groups (Fig. 16.2d). Since PPV is insoluble, typically derivatives such as MEH-PPV[1] [972] that are soluble in organic solvents are used. Compared to benzene, the substitution of one carbon atom by nitrogen (pyridine) represents doping with one electron. In Fig. 16.3, the most important building blocks of organic molecules are shown.

16.1.2 Organic Semiconductor Crystals

Small organic molecules can crystallize into solids, so-called *organic molecular crystals* (OMC), due to van-der-Waals interaction. In Fig. 16.4a, the monoclinic unit cell of an anthracene crystal [973] is shown as an example.

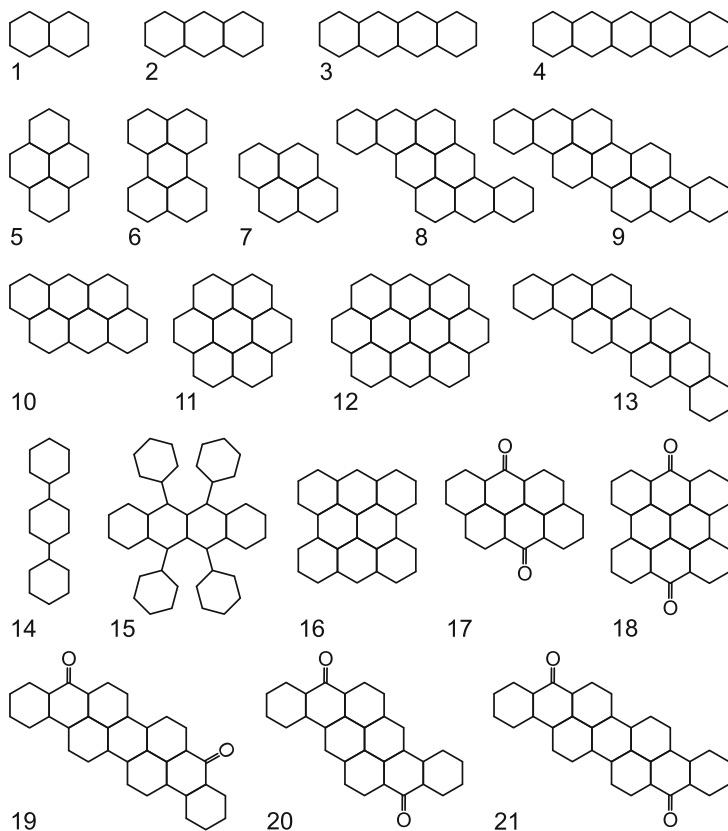[1] 2-ethoxy,5-(2'-ethyl-hexyloxy)-1,4-phenylene vinylene

Fig. 16.1. Various organic compounds: 1: naphthalene, 2: anthracene, 3: tetracene, 4: pentacene, 5: pyrene, 6: perylene, 7: chrysene, 8: pyranthrene, 9: isoviolanthrene, 10: anthanthrene, 11: coronene, 12: ovalene, 13: violanthrene, 14: p-terphenyl, 15: rubrene, 16: m-dinaphthanthrene, 17: anthanthrone, 18: m-dinaphthanthrone, 19: violanthrone, 20: pyranthrone, 21: isoviolanthrone

Also tetracene and pentacene (Fig. 16.4b) have this layered 'herringbone' structure. A comparison of the unit cells of oligoacene crystals is given in Table 16.1.

Crystal growth of single crystal OMC is achieved with a variety of methods, among them sublimation, Bridgman- and Czochralski-type methods [974, 975], vapor phase growth [976, 977] or from solution [978, 979]. Single organic molecular crystals exhibit intrinsic material properties. The practical use of organic semiconductors involves thin films, e.g. in LEDs (OLED, Sect. 22.3.7) and transistors (OFET, Sect. 23.6.3). Thin films of organic molecules are typically disordered and their performance parameters are inferior to that of OMCs.
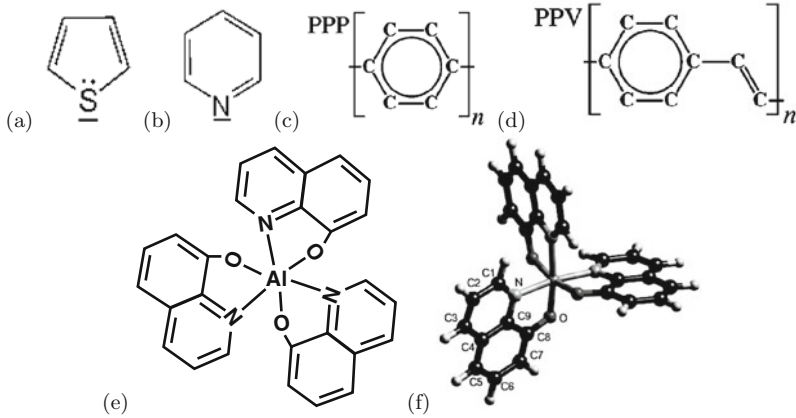
Fig. 16.2. Organic compounds: (**a**) thiophene, (**b**) pyridine, (**c**) poly-(p-phenyl), (**d**) poly-(p-phenylvinyl), (**e**) Alq$_3$ (tris-(8-hydroxyquinolate)-aluminum) and (**f**) a three-dimensional view of the Alq$_3$ molecule. Part (**f**) reprinted with permission from [980], ©1998 AIP
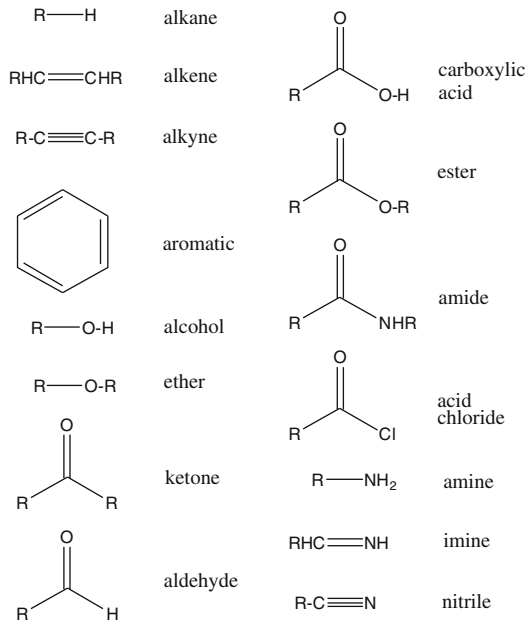

Fig. 16.3. Building blocks of organic molecules, 'R'=alkyl group, i.e. CH$_3$ (methyl-), CH$_3$CH$_2$ (buthyl-), ...
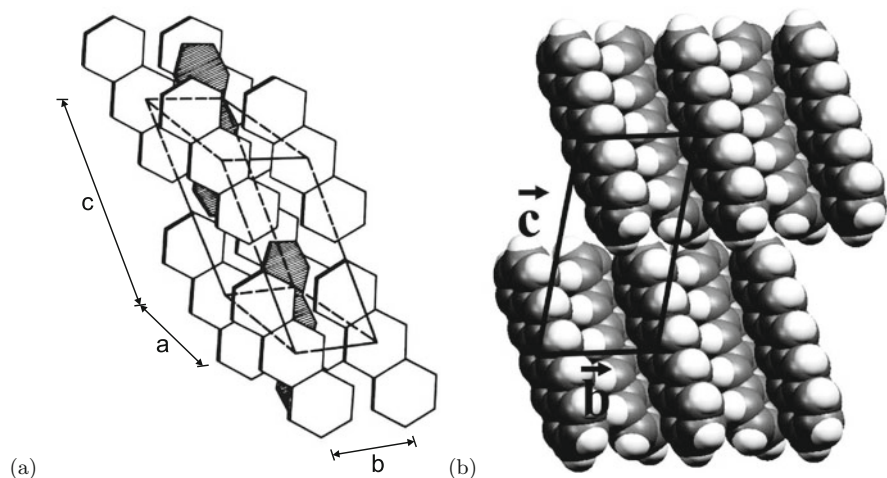
Fig. 16.4. (a) Monoclinic unit cell (for size see Table 16.1) of anthracene crystal. (b) Two herringbone layers of pentacene in a projection onto the bc plane of the triclinic unit cell. Adapted from [982]

Table 16.1. Properties of oligoacene crystals. Melting point and unit cell parameters. Data from [983]

property	naphthalene	anthracene	tetracene	pentacene
melting point (°C)	80	217	357	$> 300°$C
crystal system	monoclinic	monoclinic	triclinic	triclinic
a (nm)	0.824	0.856	0.798	0.793
b (nm)	0.600	0.604	0.614	0.614
c (nm)	0.866	1.116	1.357	1.603
α (°)	90	90	101.3	101.9
β (°)	122.9	124.7	113.2	112.6
γ (°)	90	90	87.5	85.8

16.2 Electronic Structure

The p_z orbitals in benzene are partially filled and there is an energy gap between HOMO and LUMO (Fig. 2.11). A similar consideration is valid for polymers. The coupling of orbitals along the polymer chain leads to broadening of the π and π^* states into a (filled) valence and an (empty) conduction band, respectively (Fig. 16.5). The HOMO and LUMO positions of various organic semiconductors are shown in Fig. 16.6 relative to the vacuum level (cmp. Fig. 11.14 for inorganic semiconductors). The HOMO is also known
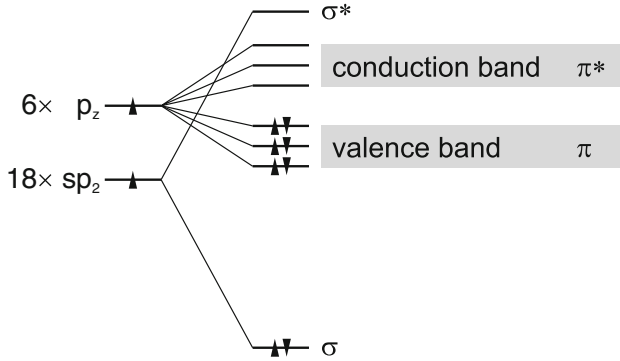
Fig. 16.5. Schematic band structure of a polymer originating from the states of the benzene molecule (see Fig. 2.11)

as *ionization energy* (IE), the LUMO as *electron affinity* (EA). With layered organic semiconductors heterostructures can be built, e.g. to design recombination pathways (recombination layer, electron blocking layers (EBL) and hole blocking layers (HBL)). For electron injection and electron extraction (hole injection) contacts, metals with appropriate work function (in connection with a possible interface dipole layer) have to be used. More details on injection and extraction contacts to organic semiconductors are discussed in Sect. 20.2.7.
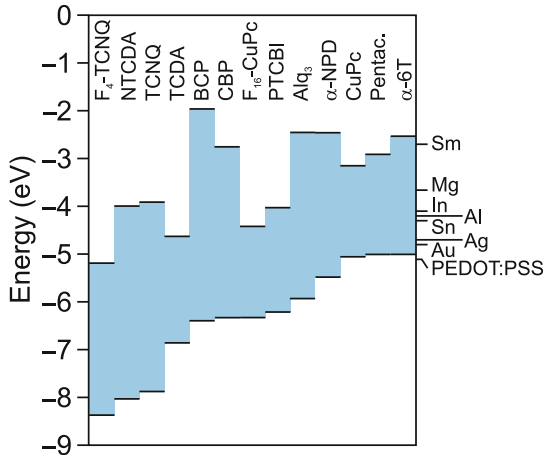

Fig. 16.6. Position of HOMO and LUMO for a variety of organic semiconductors (relative to a common vacuum level at $E = 0\,$eV). Based on values from [983]. On the right hand side the work functions of several metals are shown for comparison

16.3 Doping

The doping of organic semiconductors can be achieved by

– partial oxidation or reduction of the organic molecule,
– substitution of atoms in the organic molecule,
– mixing of the matrix with 'dopant' molecules.

The systematic shift of the Fermi level with dopant concentration has been reported in [985]. Typically, the conductivity increases superlinearly with the doping concentration (Fig. 16.7a), an effect discussed in detail in [986]. While the mobility remains constant, the thermal activation energy E_a for carriers decreases with increasing doping (Fig. 16.7b) due to electrostatic interaction [421, 987], an effect already discussed in Sect. 7.5.6. The activation energy in the dilute limit $E_{a,0}$ is modified to (cmp. (7.58))
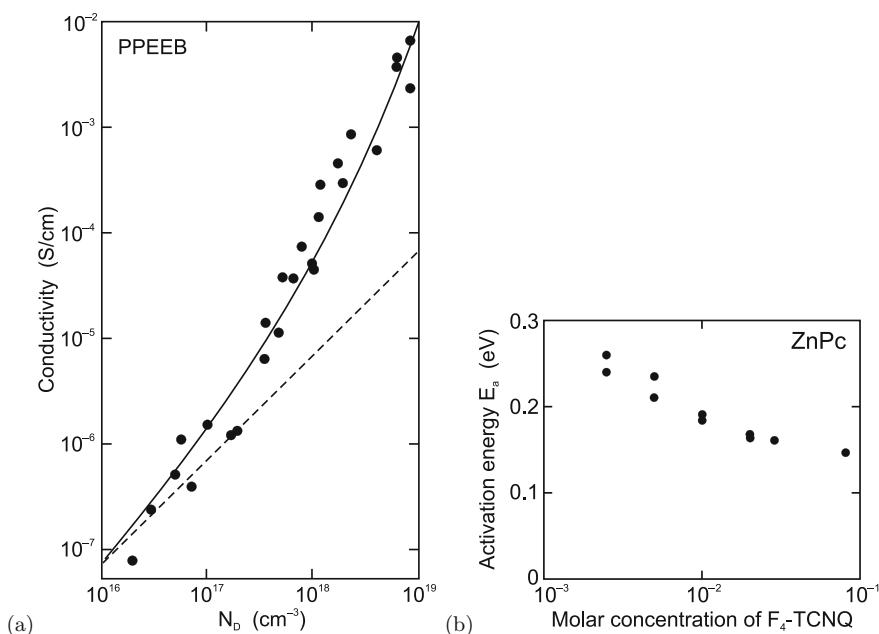
$$E_a = E_{a,0} - \beta\, N_D^{1/3} \; . \tag{16.1}$$

Fig. 16.7. (**a**) Conductivity (at $0.9\,\mathrm{V/\mu m}$) vs. dopant concentration N_D for PPEEB films. Experimental data (*circles*) and fit (*solid line*) according to (16.1) with activation energy $E_{a,0} = 0.23\,\mathrm{eV}$ and $\beta = 6.5 \times 10^{-8}\,\mathrm{eV\,cm}$ ($\mu = 0.2\,\mathrm{cm^2/Vs}$). *Dashed line* denotes linear relation between conductivity and N_D. Adapted from [984]. (**b**) Thermal activation energy E_a of carriers (holes) in ZnPc:F$_4$-TCNQ as a function of the molar dopant concentration. Adapted from [985]

16.4 Transport Properties

Transport in organic semiconductors is characterized by

– strong polaronic effects,
– hopping conduction,
– low mobility, low drift saturation velocity.

The interaction of charges with lattice deformations leads to the formation of polarons [988]. In organic materials these are often 'small', i.e. the extension of the deformation is on atomic scale. Such self-trapping of charges reduces their mobility. Two charges can share the same deformation (bipolaron) or oppositely charged polarons can attract (similar to an exciton). If these charges are on the same (neighboring) polymer chain, the polaron is called intrachain (interchain).

The conductivity within a molecule, e.g. a long polymer chain, and the conductivity between different molecules have to be distinguished. The conduction between different molecules occurs via *hopping*. Typically, the conductivity is thermally activated according to

$$\sigma = \sigma_0 \, \exp\left(-\frac{E_\mathrm{a}}{kT}\right) \; , \tag{16.2}$$

where E_a is an energy of the order of $1\,\mathrm{eV}$. Such activation also pertains to the mobility alone, e.g. $E_\mathrm{a} = 0.48\,\mathrm{eV}$ for PPV [989]. The maximum low-field mobility of many crystalline organic semiconductors at room temperature is around $1\,\mathrm{cm}^2/\mathrm{Vs}$ with a weak temperature dependence [990]. Such mobility is much smaller than that of crystalline silicon AND rather comparable to that of amorphous silicon. Improved purity and handling of organic semiconductors has allowed to achieve intrinsic material properties (Fig. 16.8). The mobility increases at low temperatures, e.g. below $100\,\mathrm{K}$ in naphthalene [991]. This has been attributed to the freeze-out of phonons and the transition from hopping to band transport. The drift velocity at higher fields shows saturation but the values, even at low temperature, are much smaller than in silicon (Fig. 16.9). An analytical model for the described main features of transport in organic semiconductors has been given in [992].

16.5 Optical Properties

Organic molecules can emit light efficiently and are thus useful for light emitters. For the photo-physics of organic materials it is essential to recall the molecular physics of singlet and triplet states. In the singlet (triplet) state, the total spin quantum number of the unpaired electrons is $S = 0$ ($S = 1$). A simple energy scheme includes a ground state S_0 and excited singlet (S_1)
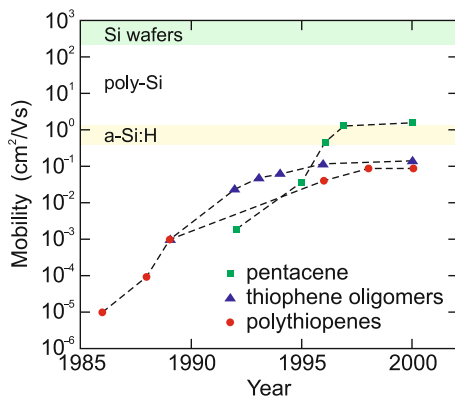
Fig. 16.8. Historic development of the experimentally achieved mobility of organic semiconductors at room temperature
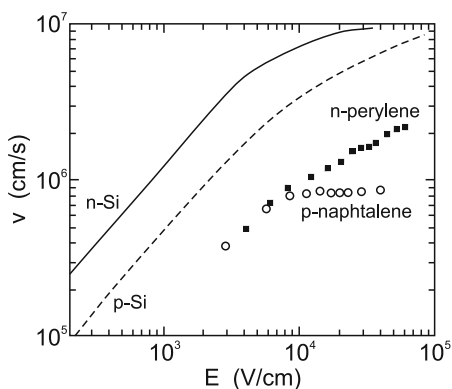

Fig. 16.9. Carrier velocity in ultrapure and highly perfect single crystals of (n-conducting) perylene at $T = 30\,\mathrm{K}$ and (p-conducting) naphthalene at $T = 4.3\,\mathrm{K}$. For comparison electron (hole) velocity in silicon at room temperature is shown as *solid* (*dashed*) line. Adapted from [975]

and triplet (T_1) states. The recombination transition $\mathrm{S}_1 \to \mathrm{S}_0$ is allowed and its lifetime short. Such luminescence is termed 'fluorescence'. Recombination from the triplet state is forbidden or at least very slow ('phosphorescence').

As an example for a small organic molecule, the fluorescence lifetime of Alq_3 is about 12 ns [993]. The triplet lifetime is in the 10 μs range [994]. Luminescence and absorption spectra of Alq_3 are shown in Fig. 16.10. The luminescence peak is redshifted with respect to the absorption edge due to the Frank-Condon principle (Fig. 10.20). The density of excited (empty) states of the Alq_3 molecule is shown in Fig. 16.11 together with the orbitals associated with the four prominent states. The lowest orbital is the LUMO and leads to the visible luminescence of the Alq_3 in the red.
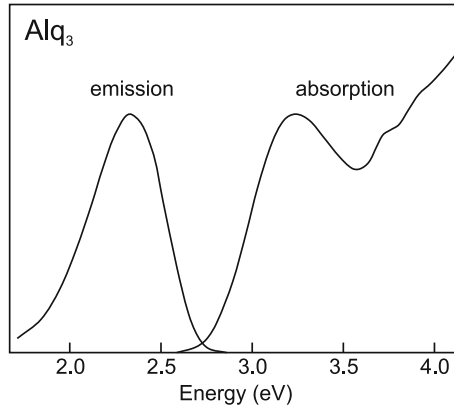
Fig. 16.10. Luminescence and absorption spectra of Alq$_3$ (vapor-deposited 150 nm thin film on a quartz substrate) at room temperature. Adapted from [995]

In Fig. 16.12a, the photoluminescence (PL) and absorption of a polymer, poly-thiophene are shown. The recombination is below the band gap of 2.1–2.3 eV on an excitonic level at 1.95 eV. There are several phonon replica whose separation of 180 meV corresponds to the C–C stretching mode. The PL excitation (PLE) spectrum of poly-thiophene demonstrates that the PL at 1.83 eV can be excited via the exciton level. The theoretical band structure of poly-thiophene is shown in Fig. 16.13a. The Brillouin zone is one-dimensional. The situation I corresponds to a single molecular chain, the situation II pertains to the chain embedded in a medium with a dielectric constant $\epsilon = 3$. The predicted band gaps are 3.6 eV and 2.5 eV, respectively. The exciton binding energy is about 0.5 eV. The exciton is a Frenkel exciton that has
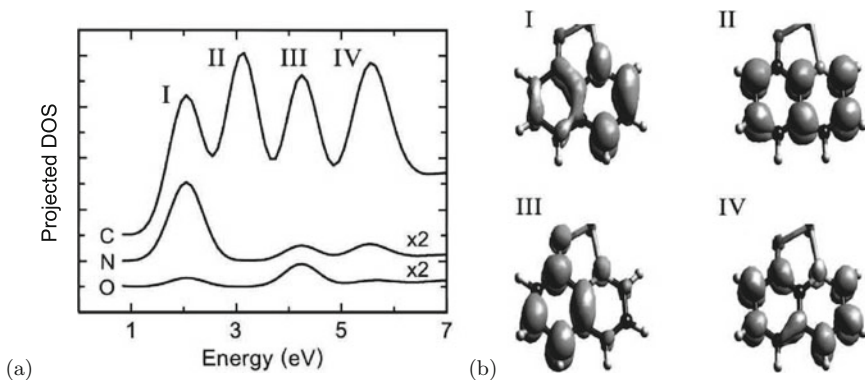

Fig. 16.11. (**a**) Projected density of states (for C, N, and O) of excited states in an Alq$_3$ molecule. The origin of the energy axis is the HOMO level. (**b**) Orbitals for the four states labeled I–IV in (**a**). Reprinted with permission from [980], ©1998 AIP

a small extension and is localized. The high binding energy is favorable for
radiative recombination since the exciton is stable at room temperature. For
photovoltaic applications, it is unfavorable since it has to be overcome in or-
der to separate electrons and holes (after absorption). Generally, intrachain
excitons (as here) and interchain excitons, where electron and the hole are
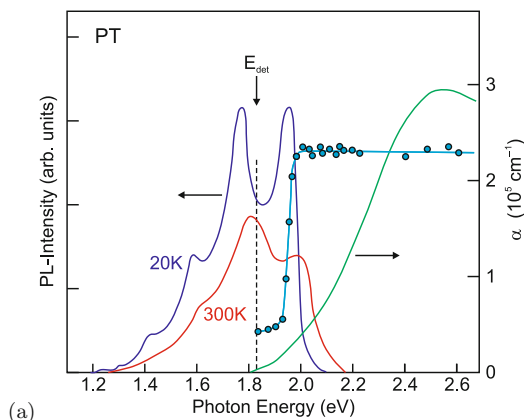localized on different chains, are distinguished.

(a)

Fig. 16.12. Photoluminescence (PL) spectra at $T = 20$ and 300 K and absorption
spectrum (*green line*) of poly-thiophene. The *vertical dashed line* denotes the de-
tection energy ($E_{\mathrm{det}} = 1.83$ eV) of the PL excitation (PLE) spectrum (*blue circles*)
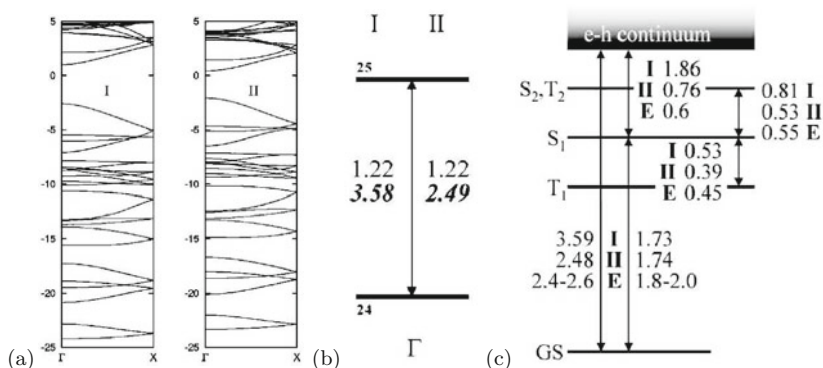($T = 20$ K). Adapted from [996]

Fig. 16.13. (**a**) Band structure of poly-thiophene ('I': naked chain, 'II': chain in a
dielectric medium ($\epsilon = 3$)), (**b**) single-particle energies and band gap, (**c**) exciton
levels ('E': experimental values). Reprinted with permission from [997], ©2002 APS

Collection of carriers in the 'dark' triplet state poses a problem limiting the quantum efficiency to 25% in a simple model [998]. Harvesting luminescence from *all* exciton states would yield significantly higher efficiencies than is possible in purely fluorescent materials (or devices).

A successful route is the use of a phosphorescent guest material. Radiative transitions from triplet states become partially allowed when the excited singlet and triplet states are mixed. This is typically achieved in metalorganic molecules with heavy metal atoms, providing large spin-orbit interaction effects [1001, 1002]. Most prominently Ru-, Pt- and Ir-containing compounds are used, e.g. *fac* tris(2-phenylpyridine) iridium [Ir(ppy)$_3$] in 4,4'-N,N'-dicarbazole-biphenyl [CBP] (Fig. 16.14a,b) [1000]. The luminescence spectrum of Ir(ppy)$_3$ is shown in Fig. 16.14d. The radiative decay constant of the Ir(ppy)$_3$ triplet state is about 800 ns and observable if energy transfer from the host triplet state is exotherm ($\Delta G = G_{\mathrm{G}} - G_{\mathrm{H}} < 0$ [994], see Fig. 16.15a) and fast. This is the case for CBP:Ir(ppy)$_3$ (Fig. 16.15b), $\Delta G \approx -0.2$ eV. Actually, reverse transfer from Ir(ppy)$_3$ to CBP seems responsible for some loss in luminescence efficiency and the decrease in phosphorescent lifetime from 800 ns to 400 ns. In the case of N,N'-diphenyl-N,N'-bis(3-methylphenyl)-[1,1'-biphenyl]-4,4'-diamine [TDP] (Fig. 16.14c) host, the triplet energy transfer to the phosphorent Ir(ppy)$_3$ guest is endotherm ($\Delta G \approx +0.1$ eV) and represents the rate limiting step [994]. In this case the
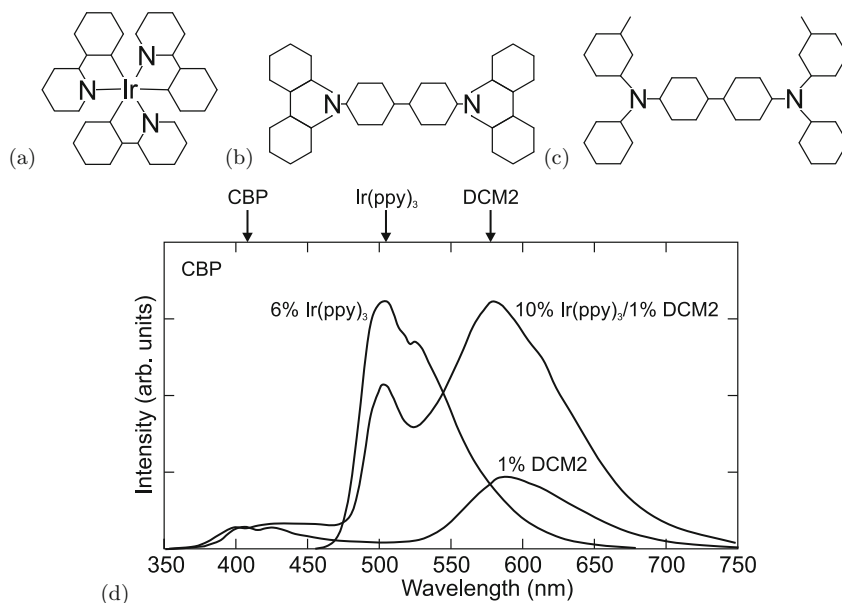

Fig. 16.14. Molecular structure of (**a**) Ir(ppy)$_3$, (**b**) CBP and (**c**) TDP (see text). (**d**) Electroluminescence spectra (at room temperature) of CBP:6% Ir(ppy)$_3$, CBP:10% Ir(ppy)$_3$/1%DCM2 and CBP:2%DCM2. Based on data from [999, 1000]
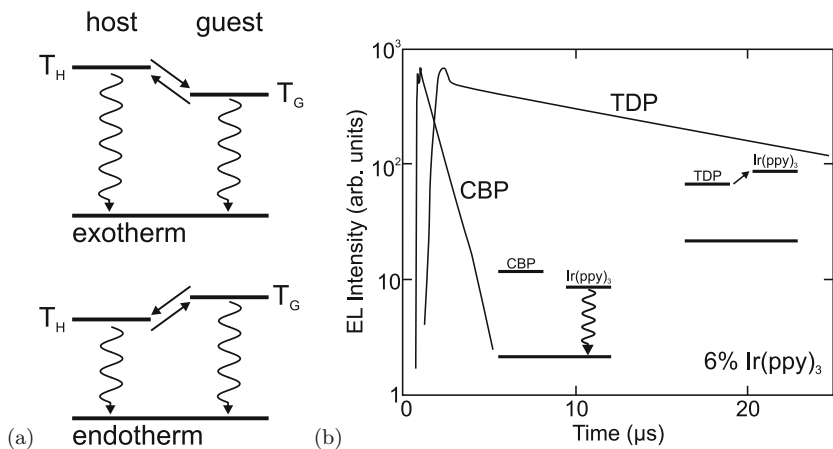
Fig. 16.15. (**a**) Schematic term diagram of host (T_H) and guest (T_G) triplet states. *Straight arrows* denote energy transfer between triplet states, *wiggly arrows* denote radiative transitions to the (singlet) ground state. (**b**) Electroluminescence transients (at room temperature, detected in the range 500–560 nm [cmp. Fig. 16.14b]) of CBP:6% Ir(ppy)$_3$ ($\tau \approx 1\,\mu$s) and TDP:6% Ir(ppy)$_3$ ($\tau \approx 15\,\mu$s). *Insets*: term schemes with arrow denoting the rate limiting step. Based on data from [994]

recombination of Ir(ppy)$_3$ has a decay constant of about 15 µs (Fig. 16.15b). The thermal activation character is confirmed by even longer decay times at low temperatures ($\tau \approx 80\,\mu$s at $T = 200$ K) [994]. Endothermic transfer allows to pump a blue guest phosphor without a blue host material.
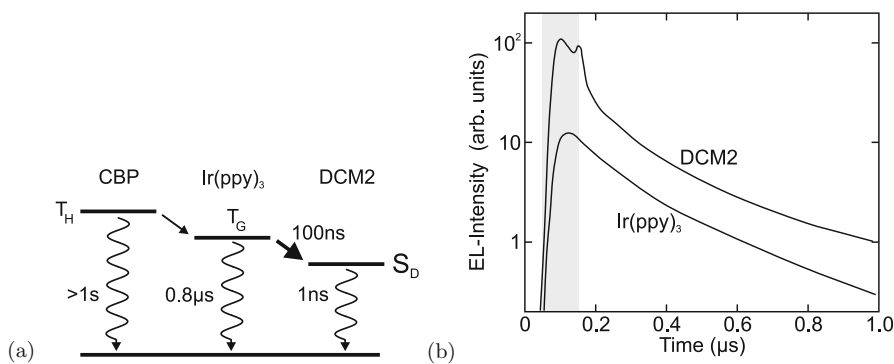

Fig. 16.16. (**a**) Schematic term scheme of CBP:Ir(ppy)$_3$/DCM2 and energy transfer and recombination paths (cmp. spectrum in Fig. 16.14). The rate constants are shown for various processes, the rate limiting step is shown with a *bold arrow*. (**b**) Electroluminescence transients after 100 ns excitation pulse (*grey area*) of Ir(ppy)$_3$ and DCM2 luminescence from CBP:10% Ir(ppy)$_3$/1% DCM2. Based on data from [999]
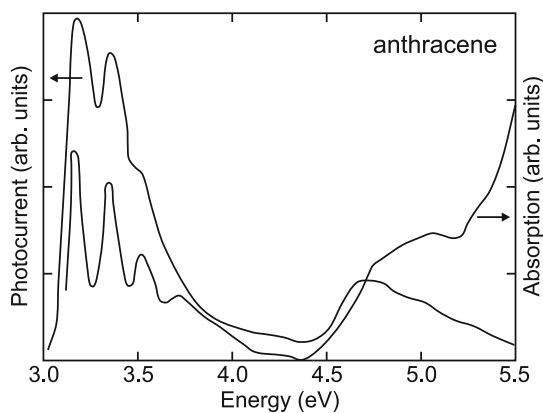
Fig. 16.17. Photoconductivity and absorption spectrum of anthracene

Further, subsequent Förster energy transfer [1003] from the guest triplet state to a fast and efficient singlet state (S_D) of a fluorescent dye is possible, e.g. from CBP:Ir(ppy)$_3$ to DCM2 [999]. The transient lifetime of pure DCM2 is about 1 ns. In a mixture of CBP:10% Ir(ppy)$_3$/1% DCM2 the luminescence of DCM2 appears with the same 100 ns decay constant as that of Ir(ppy)$_3$ (Fig. 16.16b). This decay constant (rate limiting step, see Fig. 16.16a) corresponds to the energy transfer depleting the triplet state of Ir(ppy)$_3$ to DCM2 and is much faster than the pure Ir(ppy)$_3$ radiative lifetime.

The photoconductivity of organic semiconductors is typically related to their absorption spectrum as shown for anthracene in Fig. 16.17.